

# Behavior of sphingomyelin and ceramide in a tear film lipid layer model

Agnieszka Olżyńska<sup>1</sup> and Lukasz Cwiklik<sup>1,2,\*</sup>

<sup>1</sup>J. Heyrovský Institute of Physical Chemistry, Academy of Sciences of the Czech Republic, v.v.i., Dolejškova 3, Prague, 18223, Czech Republic

<sup>2</sup>Institute of Organic Chemistry and Biochemistry, Academy of Sciences of the Czech Republic, Flemingovo nám. 2, Prague, 16610, Czech Republic

\*corresponding author: lukasz.cwiklik@jh-inst.cas.cz (L.C.)

## Abstract

Tear film lipid layer is a complex lipid mixture forming the outermost interface between eye and environment. Its key characteristics, such as surface tension and structural stability, are governed by the presence of polar lipids. The origin of these lipids and exact composition of the mixture are still elusive. We focus on two minor polar lipid components of the tear film lipid layer: sphingomyelin and ceramide. By employing coarse grain molecular dynamics *in silico* simulations accompanied by Langmuir balance experiments we provide molecular-level insight into behavior of these two lipids in a tear film lipid layer model. Sphingomyelin headgroups are significantly exposed at the water-lipids boundary while ceramide molecules are incorporated between other lipids frequently interacting with nonpolar lipids. Even though these two lipids increase surface tension of the film, their molecular-level behavior suggests that they have a stabilizing effect on the tear film lipid layer.

## Keywords

Tear film lipid layer; Molecular dynamics simulations; Langmuir balance; Sphingomyelin; Ceramide

## Introduction

Tear film is an aqueous layer covering cornea of human eye (Forrester et al., 2015). It forms a smooth and transparent optical surface, serves as a source of nutrients and oxygen for cornea, and forms a first line of defense against pathogens and dirt particles. The aqueous components of the tear film are secreted by lacrimal glands (Mishima et al., 1966). The outermost layer of the tear film is formed by a layer of lipids, so called tear film lipid layer (TFLL) (Butovich, 2009; Cwiklik, 2016). Its main role is to reduce surface tension of the tear film, hinder water evaporation, and help in tear film re-spreading after blinks. Alterations of TFLL composition are one of key factors responsible for occurrence of dry eye syndrome (King-Smith et al., 2013). TFLL consists of two main classes of lipids: nonpolar (or hydrophobic) and polar lipids. The first class is secreted by Meibomian glands, small glands opening at the rim of eyelids (Jester et al., 1981; McCulley and Shine, 2003). The secretion of Meibomian glands contains also 0.1 mol% of polar lipids (Millar and Schuett, 2015). The lipidomics of the whole tear film indicates that there is 5-13 mol% of polar lipids in the aqueous phase, therefore they cannot originate exclusively from the Meibomian glands. However, the source of these extra polar lipids is not known (Millar and Schuett, 2015; Pucker and Haworth, 2015). They likely originate from more than one source, for instance, they can be a cellular debris from the lacrimal or Meibomian glands (Rohit et al., 2014).

The lipidomic studies demonstrate significant variation regarding exact composition of TFLL, in particular its polar lipid fraction (see the comprehensive review in Ref. (Millar and Schuett, 2015) and references therein). Apart from technical problems regarding sample collection and some inaccuracies of lipidomic methods, there are also significant variations of lipidome between different patients as well as in individual patients depending on tear collection conditions (Brown et al.). Therefore, it is difficult to mimic physiological

composition of tear lipids in biophysical model studies and hence some proxy systems are typically used. For instance, in a combined experimental and computational study of Kulovesi et al., a mixture of egg phosphatidylcholine and free fatty acids was employed as polar lipid phase whereas the nonpolar lipid fraction was modeled by cholesteryl oleate and a mixture of triglycerides (Kulovesi et al., 2010). In our previous computational study on TFLL structural characteristics (Wizert et al., 2014) we employed a mixture of cholesteryl esters and triglycerides as nonpolar lipids while the polar components were chosen according to the lipidomic study of Rantamaki et al. (Rantamaki et al., 2011). That study showed that the polar lipids of human tears consist of phosphatidylcholines (PC), phosphatidylethanolamines (PE), sphingomyelins (SM) and ceramides (Cer).

It was suggested that TFLL typically forms a layered structure with the less abundant polar lipids separating the abundant nonpolar components from the aqueous sublayer (McCulley and Shine, 1997; Tiffany et al., 1997). Indeed, such an organization of lipids was confirmed at the molecular level in previous studies employing MD simulations (Kulovesi et al., 2012; Wizert et al., 2014). Namely, a monolayer of polar lipids residing at the water-lipid interface was observed while the nonpolar lipids formed a relatively thick coating atop of their polar counterparts with some interdigitation observed between chains of polar and nonpolar molecules.

The actual tear film is a highly dynamic system because it is disturbed by blinks, evaporation and the constant tear flow from lacrimal glands to the nasolacrimal duct (Mishima et al., 1966). At the molecular level, these disturbances can be modeled, to some extent, by varying lateral pressure of the film. MD simulations showed that under such circumstances the model TFLL can preserve its stability with polar lipid monolayer undergoing undulations and thus accommodating to the varying conditions (Wizert et al., 2014). Moreover, the restructuring of the polar sublayer can lead to formation of both

micelles and inverse micelles while still preserving TFLL structural stability. At the molecular level, the reorganization details of the polar sublayer must, at least to some extent, depend on its lipid composition. It was demonstrated in the case of lipid monolayers that system restructuring depends on the identity of lipids (Baoukina et al., 2014). Notably, in the previous simulation study of TFLL, some polar lipids, in particular SM and Cer, were spatially sorted upon TFLL undulation (Wizert et al., 2014). Ceramides in cell membranes are generated by enzymatic breakdown of sphingomyelin and it was demonstrated that the increase of Cer concentration significantly changes biophysical properties of model lipid systems by formation of ordered structures (Fanani et al., 2010; López-Montero et al., 2010). Similarly, a complex phase behavior of Cer was also demonstrated in monolayer systems (Catapano et al., 2015; Fanani et al., 2010). It may be presumed that this property can be at least partially related to the role of SM-Cer balance in cell signaling (Grassmé et al., 2007; Kolesnick et al., 2000). In the context of the TFLL it is interesting that these two lipids were detected in considerable amounts in the human tear lipidome (Rantamaki et al., 2011).

Motivated by the role of Cer and SM in cell membranes and the fact that they both are present in the tear film, we aimed at addressing in detail their molecular-level behavior in TFLL. To this end, we employed coarse grained molecular dynamics (MD) simulations of a previously introduced TFLL model and its analogues with varying polar lipids composition. The *in silico* simulations were accompanied by Langmuir trough experiments performed for polar lipid monolayers with the aim to assess the influence of the changing lipids composition on macroscopic behavior of the monolayers that form polar fraction of TFLL.

## **Material and methods**

### *MD simulations*

Classical MD simulations were employed to simulate a model of TFL. The model introduced in our previous study (Wizert et al., 2014) was employed. That model was shown to reproduce main structural characteristics of the actual TFL. It consisted of four types of polar lipids: 1-palmitoyl-2-oleoyl-phosphatidylcholine (POPC); 1-palmitoyl-2-oleoyl-phosphatidylethanolamine (POPE); N-palmitoyl-D-erythro-sphingosine (Cer); and N-palmitoyl-D-erythro-sphingosylphosphorylcholine (SM). Nonpolar lipids were represented by glycerine trioleate (TG) and cholesteryl oleate (CE). The coarse grain MARTINI force field was used for lipids (Marrink et al., 2007) with exception of Cer that was parameterized in house employing the parameters of SM lipid with the headgroup bead exchanged to the P1 MARTINI type. Periodic simulation box was used with ~87000 water beads placed in the middle of the box that was elongated in one direction to form two water-vacuum interfaces. Simulation box contained 976 POPC, 320 POPE, 80 SM, 80 Cer, 2544 TG, and 2400 CE molecules. Lateral size of the system was kept constant (see below) to allow for simulations at two values of the area per polar lipid (APPL), either 0.67 or 0.45 nm<sup>2</sup>. Two additional systems, deficient in either SM or Cer, were also simulated at both APPL values. In total, six systems were simulated.

Simulations were performed employing the GROMACS 5.0.7 software (Hess et al., 2008). A standard protocol advised for MARTINI simulations with GROMACS5 was employed. Namely, non-bonded interactions were cut-off at the distance of 1.1 nm using the potential-shift-Verlet method. The reaction-field method was used to account for long-range electrostatics with the relative electrostatic screening parameter equal 15. The time step of 20 fs was used to integrate equations of motion. The temperature of 305 K was controlled employing the velocity rescale method. This value of temperature was chosen to correspond to our earlier study (Wizert et al., 2014) whereas ~310K that we employed in experiments (see below) is closer to physiological conditions. Note, however, that in the MARTINI force

field such a temperature difference does not practically influence the simulated system. Simulations were performed within the canonical ensemble with the size of the box kept constant. Trajectories of 500 ns were calculated with first 300 ns of each simulation treated as equilibration and hence not used in analysis. Analysis of density profiles, contact, radial distribution functions, and surface tension was performed employing standard GROMACS tools ('density', 'mindist', 'rdf', and 'energy', correspondingly).

### *Langmuir balance experiments*

1-palmitoyl-2-oleyl-sn-glycero-3-phosphocholine (POPC), 1-palmitoyl-2-oleoyl-sn-glycero-3-phosphoethanolamine (POPE), N-stearoyl-D-erythro-sphingosylphosphorylcholine (SM), and N-stearoyl-D-erythro-sphingosine (Cer) were purchased from Avanti Polar Lipids (Alabaster, AL). Phosphate buffered saline (PBS) and chloroform of spectroscopic grade were ordered from Sigma-Aldrich (St. Louis, MO, USA). The buffer was prepared using Milli Q water (Milipore, USA). All chemicals were used without further purification.

Langmuir monolayer measurements were performed on a commercially available MicroTrough setup with all-Teflon trough (maximum surface area of 12331mm<sup>2</sup>) (μtrough XS, Kibron; Helsinki, Finland). The system was equipped with ultra-sensitive surface pressure sensor (KBN 315; Kibron) with the DyneProbe. The appropriate volume of 1 mM solution of lipid mixture in chloroform was spread onto a trough filled with 10 mM PBS (0.137 M NaCl, 0.0027 M KCl, pH 7.4) with a Hamilton microsyringe. Surface pressure-molecular area ( $\pi$ -A) isotherms were collected during the symmetrical movement of two Teflon barriers controlled by software (FilmWare) provided by the equipment manufacturer. The compression speed was 5 mm/min (or 1.96 Å<sup>2</sup>/chain/min). Measurements were done at the temperature of 310 K that was controlled with a temperature control plate (connected to water-circulating thermostat;  $\pm$  0.5 K accuracy) placed under the trough. To slow down subphase evaporation and protect from dust and additional surface disruptions, an acrylic cover box over the trough was used. Before each measurement the monolayer was left uncovered for 7 min to allow chloroform to evaporate and then for 10 min covered with the acrylic box to allow temperature to equilibrate.

## Results and Discussion

### *Localization of SM and Cer in the TFLL model*

The TFLL structure and hence its properties are governed by spatial organization of lipids at the water-air interface. MD simulations, due to their molecular resolution, provide us with direct insight into organization of the lipid film. Moreover, a role of individual components, in particular the minor ones, can be analyzed. Representative snapshots of laterally relaxed (APPL=0.67 nm<sup>2</sup>) and compressed (APPL=0.45 nm<sup>2</sup>) POPC/POPE/SM/Cer systems obtained in MD simulations upon equilibration are presented in Fig. 1. In the case of the relaxed lipid film, a three-layer structure of the TFLL is observed. Namely, polar lipids accumulate at the interface between water and lipids forming a monolayer. Nonpolar lipids, on the other hand, reside atop of the polar monolayer thus creating a thick multilayer in contact with polar lipids at one side, and with the air at the other. In the case of the laterally compressed film, the TFLL restructures forming stable undulations. Notably, in the case of the relaxed film, some structural features of the polar monolayer can be distinguished by visual analysis of simulation snapshots (Fig. 1). Specifically, SM headgroups are mostly protruding through headgroups of POPC whereas Cer molecules are predominantly residing in the interior of the monolayer, hidden in between other lipid molecules. These structural features can be quantified employing density profiles calculated across the interface. In Fig. 2, density profiles of selected system components at APPL=0.67 nm<sup>2</sup> are presented. As visible in Fig. 2a, the headgroups of SM are clearly the most exposed to the water phase, more than the headgroups of POPC. Note that both POPC and SM have the same phosphatidylcholine (PC) moiety as their headgroup. This supports the previous observation based on the simulation snapshots that SM headgroups protrude toward the water phase through the POPC. The headgroups of POPE are somewhat hidden by POPC, this is because

the phosphoethanolamine (PE) group is smaller than PC and hence fits in-between PCs. Finally, headgroups of Cer formed by the hydroxyl moiety are the least exposed to the water phase; this can be rationalized by their small size. Regarding acyl chains, both POPC and POPE terminals are the most exposed to nonpolar lipids. On the other hand, SM is the least exposed, this is because whole molecules of SM are shifted toward the water phase. Presentation of Cer at the polar-nonpolar boundary is also limited, most likely due to the relatively short length of the sphingosine chain.

Some structuring occurs also within the nonpolar lipid phase, more specifically, at the polar-nonpolar interface, see Fig. 2b. Regarding CE, its C3-chain (oleate) together with the ring system penetrates in-between acyl chains of phospholipids. The C17-chain of CE also penetrates into the polar monolayer, although to a lesser extent. A visual inspection of the trajectories reveals that this is because the cholesterol moiety of CE is able to reside in-between polar lipids in two orientations, with its oleate chain pointing either toward water or non-polar phase. Note that in particular the latter orientation, even though less abundant, resembles the typical orientation of cholesterol in phospholipid bilayers. Thus, some similarities with lipid bilayers regarding cholesterol ring-lipid interactions can be expected; this issue will be addressed in the following sections. Acyl chains of TG are also able to penetrate in between chains of polar lipids but significantly less than those of CE.

Note that for the undulated lipid film under lateral compression, density profiles cannot be easily used to analyze positioning of lipids in the TFL. Nevertheless, based on visual inspection of the trajectory at APPL=0.45 nm<sup>2</sup>, similar trends regarding presentation of SM headgroup and burying of Cer occur.

*Lipid-lipid interactions – lateral inhomogeneities*

Multi-component lipid monolayers and bilayers often exhibit lateral inhomogeneities due to non-ideal lipid mixing (Baoukina et al., 2014). Lateral structural integrity of a film, in particular its durability under lateral compression and decompressions as experienced by TFLL, would be diminished in a presence of significant structural non-idealities. To examine the lateral mixing in the TFLL model we analyze contacts between individual lipid types. In Fig. 3, average number of contacts of polar lipids per one POPC molecule are presented at APPL=0.67 nm<sup>2</sup>. Two lipid molecules were considered to be in contact if any of MARTINI beads representing atom groups in one of the molecules was at the distance below the assumed cutoff from a bead of the other molecule. The analysis was performed employing the Gromacs “mindist” tool with the option “-group” and the default 0.6 nm cutoff. The data show small heterogeneities in lipid mixing. Namely, POPC-POPC contacts prevail, followed by POPC-POPE and then POPC-SM and POPC-Cer. Note that regarding SM and Cer, there is somewhat more (~4%) POPC-SM contacts (5.3 per a POPC molecule) than POPC-Cer (5.1). Virtually the same results are observed at APPL=0.45 nm<sup>2</sup> (see supplementary Fig. S1). These local (~1 nm) non-idealities of lipid mixing, however, do not propagate to larger length-scales. Namely, as revealed by means of lateral radial distribution functions (see supplementary Fig. S2), the TFLL does not exhibit any particular lateral preferences or ordering at long distances. Overall, no significant heterogeneities of lipid mixing or lateral organization were observed. In other words, neither of the polar lipids in the considered TFLL model has particular tendency to de-mix or form laterally organized domains; it results in laterally homogeneous lipid film.

### *Lipid hydration*

The water-TFLL interface is formed by headgroups of polar lipids, as was evidenced by density profiles (Fig. 2). To further quantify interactions between water and lipids, we analyzed the number of contacts between water and polar lipid headgroups. The overall number of contacts (shown in supplementary Fig. S3) is a function of lipid concentration and hence water-POPC contacts prevail, followed by these of water-POPE. Interestingly, SM makes more contacts with water than Cer, even though their concentrations in the film are equal. Lateral compression of the TFLL leads to general reduction of water-lipid contacts, this can be intuitively explained as “squeezing-out” of water from the compressed film. More insight into water-lipid binding preferences can be gained while analyzing water contacts per an individual headgroup. In Fig. 4, average number of contacts of water beads made per one lipid headgroup are presented at both APPL=0.67 and 0.45 nm<sup>2</sup>. Contacts between water and SM evidently dominate with on average ~9 water beads per one SM. Both POPC and POPE headgroups are less hydrated than SM, the latter most likely due to its small size. Contacts with water are the least abundant in the case of Cer headgroups. Lateral compression to APPL=0.45 nm<sup>2</sup> leads to overall reduction of water-lipid contacts. This effect is, however, the smallest in the case of SM thus showing that the well hydrated PC moiety of SM is well exposed to the water phase also in the undulated TFLL. Note that in contrast to the density profiles, the hydration analysis is valid for the undulated lipid film at APPL=0.45 nm<sup>2</sup>. The results of the hydration analysis correspond directly with presentation of the polar headgroups evidenced by density profiles (Fig. 2). The well exposed toward water phosphatidylcholine headgroups of SM are hydrated more than their POPC counterparts. The relatively small headgroups of POPE are less hydrated than POPC, but still more than the smallest and hidden in-between other lipids headgroups of Cer.

*Interactions of polar lipids with cholesteryl ester*

As noted beforehand, the cholesterol moiety of cholesteryl ester penetrates relatively deep into the polar lipids sublayer. In principle, it can interact with acyl chains of lipids, similarly to how cholesterol does in lipid bilayers. Fig. 5 shows average number of contacts between a lipid molecule and molecules of cholesteryl ester at APPL=0.67 and 0.45 nm<sup>2</sup>. Contacts with CE are the most frequent in the case of POPE, with POPC being the next interaction partner. Regarding Cer and SM, the former creates more contacts than SM but both are less frequent CE contact partners than POPC and POPE. This is somewhat surprising as SM and Cer molecules are based on the sphingosine unit which is supposed to favoring interactions with cholesterol in bilayers (Björkbom et al., 2010; Castro et al., 2009; Róg and Pasenkiewicz-Gierula, 2006). The somewhat higher number of Cer-CE contacts can be rationalized by position of Cer deeper in the polar monolayer, hence farther from water and closer to the non-polar lipid sublayer. On the other hand SM, as being the most exposed to water, is interacting with non-polar lipids the least frequent. At APPL=0.45 nm<sup>2</sup>, contacts with CE change. Namely, Cer and POPE have more frequent encounters with CE, SM-CE contacts are reduced, while POPC-CE contact are virtually unchanged. This points to possible repositioning of both Cer and POPE toward the non-polar phase during lateral compression of TFLL, and shifting of SM toward the water phase.

#### *Influence of SM and Cer on surface tension*

The molecular-level features of the TFLL described above are a basis for longer-range properties of the film, such as surface tension, which can be compared with experimental values. In order to analyze the influence of SM and Cer on the surface tension of the TFLL, apart from the TFLL model with four polar lipids, we considered two auxiliary

systems, deficient in either Cer or SM (POPC/POPE/SM and POPC/POPE/Cer, accordingly). In Fig. 6, surface tension calculated in the course of MD simulations in the three considered systems under both laterally relaxed and compressed conditions is presented. In the case of the laterally relaxed lipid films, the absence of both SM and Cer leads to increase of surface tension. The effect is more pronounced in the case of SM-deficient system. In other words, SM causes stronger reduction of surface tension than Cer. However, the system with both SM and Cer present exhibits even lower surface tension than the systems containing only one of these lipids.

The reduction of surface tension is virtually not observed in the laterally compressed systems. This can be rationalized by the fact that in the undulated film, lateral pressure, and hence surface tension, are governed by the presence of undulations and to a lesser extent by properties of individual lipid classes.

The above trends in surface tension alterations in the presence and absence of SM and Cer observed in MD simulations directly correspond with the results obtained for the mixed polar lipid monolayers during Langmuir trough measurements, as will be discussed in the next chapter.

#### *Langmuir balance experimental measurements*

In order to better understand the role of SM and Cer in the polar layer of TFLL, Langmuir balance measurements were performed for mixed polar lipid films composed of polar tear lipids at the physiologically relevant temperature of 310 K. Note that these polar lipid films under typical conditions form monolayers at the water-air interface because they are deficient in non-polar lipids present in the multilayer TFLL. Nevertheless, it can be

assumed that polar lipid monolayers are sensible models of the polar sublayer of TFLL, well suited for typical Langmuir balance experiments.

Surface pressure–molecular area ( $\pi$ -A) isotherms were recorded for POPC/POPE/SM/Cer mixtures at different ratios of SM and/or Cer to POPC in the system. The  $\pi$ -A isotherms of 12.2/4/0/0, 12.2/4/1/1, 12.2/4/1/0, and 12.2/4/0/1 POPC/POPE/SM/Cer monolayers are shown in Fig. 7. Note that the quaternary mixture (POPC/POPE/SM/Cer) corresponds to the TFLL lipidomics (Rantamaki et al., 2011) as well as to the polar lipid composition of the TFLL model employed in MD simulations. The ternary mixtures were chosen to mimic the system deficient in either SM or Cer. Additionally, the isotherm of pure POPC is presented. For all compositions measured isotherms are shifted to the left comparing to pure POPC. Taken into account the resolution of the experiment, the isotherms of POPC/POPE, POPC/POPE/SM/Cer, and POPC/POPE/SM mostly overlap, with small deviations occurring only at low APPL. On the other hand, the POPC/POPE/Cer isotherm is slightly shifted to the left with respect to all other systems for most APPL values. These results demonstrate that all mixed systems are characterized by somewhat higher surface tension (resulting from lower surface pressure) than the POPC monolayer. This includes the physiologically relevant POPC/POPE/SM/Cer quaternary system.

Since the differences in isotherm positions for compositions of monolayers described above were rather small, additional isotherms were measured for monolayers with higher ratios of SM and/or Cer to POPC in order to enhance the observed effects. For comparison isotherms for pure SM and Cer monolayers were also measured. The results are presented in Fig. 8. With respect to the POPC/POPE mixture, exchange of POPC to either SM or Cer shifts the corresponding isotherms to the left, hence increases surface tension. This effect is small in the case of ternary mixture with SM (POPC/POPE/SM) but it is clearly above the resolution of the experiment (in contrast to the tiny shifts observed in Fig. 7). The left-shift of

the isotherm is significantly more pronounced for the system containing Cer (POPC/POPE/Cer). The observed alterations of isotherms can be rationalized when pure SM and Cer systems are considered. The isotherm of the pure SM film is shifted to the left with respect to the POPC/POPE system. Similar but significantly stronger shift is observed in the case of pure Cer film. Both isotherms of one-component systems are in agreement with previously published data (Catapano et al., 2015; Vaknin et al., 2001). Note that the isotherm of SM exhibits irregular shape due to phase transitions (Vaknin et al., 2001). No such features were observed in the isotherms of the considered mixed films. The pure Cer isotherm differs significantly from all other cases. This is because of relatively small size of Cer molecules and complex phase behavior of the Cer film, as has been reported previously (Catapano et al., 2015).

The experimental results demonstrate that physiologically relevant polar lipids film has higher surface tension than the POPC monolayer. This increase is caused partially by relatively abundant POPE but also by the minor components SM and Cer. In particular, the effect of Cer is well pronounced.

## **Conclusions**

Polar lipids play essential role in the tear film lipid layer as they spread at the water-lipid boundary separating the abundant nonpolar lipids from the aqueous subphase. Here, we focused on molecular-level behavior of sphingomyelin and ceramide, two minor polar lipids of the human TFLL. Although both lipids are based on the sphingosine unit, the dissimilarity of their headgroups leads to different behavior in the lipid film. Namely, at the molecular level, SM protrudes through the headgroups of PC and PE lipids and it is well exposed to the water phase. In contrast, Cer molecules are well incorporated between other lipids and hence mostly separated from the water phase. At the same time, they readily interact with nonpolar

cholesteryl ester molecules. These characteristics of SM and Cer behavior in the TFL are further amplified under increased lateral pressure. At the macroscopic level, the presence of both SM and Cer in the polar lipid film leads to increase of surface tension. This effect can be rationalized by the fact that upon lateral compression both molecules change their position in the TFL and such a restructuring of the film reduces lateral pressure. It can be postulated that the ability to rearrange and to readily interact with water and nonpolar lipids, accordingly in the case of SM and Cer, leads to enhanced structural stability of the TFL under dynamic physiological conditions. Such an effect, apart from being important for a better understanding of tear film biophysics, can be also potentially used in a treatment of TFL-related eye ailments.

## **Appendix A. Supplementary data**

Supplementary data associated with this article can be found, in the online version, at <http://dx.doi.org/XX.XXXX/j.aanat.XXXX.XX.XXX>.

## **Acknowledgements**

This work was supported by grant 15-14292S from the Czech Science Foundation. The authors gratefully acknowledge the support of Prof. Martin Hof. Access to computing and storage facilities owned by parties and projects contributing to the National Grid Infrastructure MetaCentrum provided under the program "Projects of Projects of Large Research, Development, and Innovations Infrastructures" (CESNET LM2015042), is greatly appreciated.

## **References**

Baoukina, S., Rozmanov, D., Mendez-Villuendas, E., Tieleman, D.P., 2014. The mechanism of collapse of heterogeneous lipid monolayers. *Biophys. J.* 107, 1136-1145.

Bjorkbom, A., Rog, T., Kaszuba, K., Kurita, M., Yamaguchi, S., Lonnfors, M., Nyholm, T.K.M., Vattulainen, I., Katsumura, S., Slotte, J.P., 2010. Effect of sphingomyelin headgroup size on molecular properties and interactions with cholesterol. *Biophys. J.* 99, 3300-3308.

Brown, S.H.J., Kunnen, C.M.E., Papas, E.B., de la Jara, P.L., Willcox, M.D.P., Blanksby, S.J., Mitchell, T.W., 2016. Intersubject and Interday Variability in Human Tear and Meibum Lipidomes: A Pilot Study. *Ocul. Surf.* 14, 43-48.

Butovich, I.A., 2009. The Meibomian Puzzle: Combining pieces together. *Prog. Retin. Eye Res.* 28, 483-498.

Castro, B.M., Silva, L.C., Fedorov, A., de Almeida, R.F., Prieto, M., 2009. Cholesterol-rich Fluid Membranes Solubilize Ceramide Domains. Implications for the Structure and Dynamics of Mammalian Intracellular and Plasma Membranes *J. Biol. Chem.* 284, 22978-22987.

Catapano, E.R., Lillo, M.P., Garcia Rodriguez, C., Natale, P., Langevin, D., Monroy, F., Loopez-Montero, I., 2015. Thermomechanical Transitions of Egg-Ceramide Monolayers. *Langmuir* 31, 3912-3918.

Cwiklik, L., 2016. Tear film lipid layer: A molecular level view. *Biochim. Biophys. Acta - Biomembranes* 1858, 2421-2430.

Fanani, M.L., Hartel, S., Maggio, B., De Tullio, L., Jara, J., Olmos, F., Oliveira, R.G., 2010. The action of sphingomyelinase in lipid monolayers as revealed by microscopic image analysis. *Biochim. Biophys. Acta - Biomembranes* 1798, 1309-1323.

Forrester, J.V., Dick, A.D., McMenamin, P.G., Roberts, F., Pearlman, E., 2015. *The Eye: Basic Sciences in Practice*. 4th ed. Elsevier Health Sciences.

Grassme, H., Riethmuller, J., Gulbins, E., 2007. Biological aspects of ceramide-enriched membrane domains. *Prog. Lipid Res.* 46, 161-170.

Hess, B., Kutzner, C., van der Spoel, D., Lindahl, E., 2008. GROMACS 4: Algorithms for highly efficient, load-balanced, and scalable molecular simulation. *J. Chem. Theory Comput.* 4, 435-447.

Jester, J.V., Nicolaides, N., Smith, R.E., 1981. Meibomian gland studies - histologic and ultrastructural investigations. *Invest. Ophthalmol. Vis. Sci.* 20, 537-547.

King-Smith, P.E., Bailey, M.D., Braun, R.J., 2013. Four characteristics and a model of an effective tear film lipid layer (TFLL). *Ocul. Surf.* 11, 236-245.

Kolesnick, R.N., Goni, F.M., Alonso, A., 2000. Compartmentalization of ceramide signaling: physical foundations and biological effects. *J. Cell. Physiol.* 184, 285-300.

Kulovesi, P., Telenius, J., Koivuniemi, A., Brezesinski, G., Rantamaki, A., Viitala, T., Puukilainen, E., Ritala, M., Wiedmer, S.K., Vattulainen, I., Holopainen, J.M., 2010. Molecular organization of the tear fluid lipid layer. *Biophys. J.* 99, 2559-2567.

Kulovesi, P., Telenius, J., Koivuniemi, A., Brezesinski, G., Vattulainen, I., Holopainen, J.M., 2012. The impact of lipid composition on the stability of the tear fluid lipid layer. *Soft Matter* 8, 5826-5834.

Lopez-Montero, I., Monroy, F., Velez, M., Devaux, P.F., 2010. Ceramide: from lateral segregation to mechanical stress. *Biochim. Biophys. Acta - Biomembranes* 1798, 1348-1356.

Marrink, S.J., Risselada, H.J., Yefimov, S., Tieleman, D.P., de Vries, A.H., 2007. The MARTINI force field: coarse grained model for biomolecular simulations. *J. Phys. Chem. B* 111, 7812-7824.

McCulley, J.P., Shine, W., 1997. A compositional based model for the tear film lipid layer. *Trans. Am. Ophthalmol. Soc.* 95, 79-93.

McCulley, J.P., Shine, W.E., 2003. Meibomian gland function and the tear lipid layer. *Ocul. Surf.* 1, 97-106.

Millar, T.J., Schuett, B.S., 2015. The real reason for having a meibomian lipid layer covering the outer surface of the tear film – A review. *Exp. Eye Res.* 137, 125-138.

Mishima, S., Gasset, A., Klyce, S.D., Jr., Baum, J.L., 1966. Determination of tear volume and tear flow. *Invest. Ophthalmol. Vis. Sci.* 5, 264-276.

Pucker, A.D., Haworth, K.M., 2015. The presence and significance of polar meibum and tear lipids. *Ocul. Surf.* 13, 26-42.

Rantamaki, A.H., Seppanen-Laakso, T., Oresic, M., Jauhiainen, M., Holopainen, J.M., 2011. Human tear fluid lipidome: from composition to function. *PLoS One* 6, e19553.

Rog, T., Pasenkiewicz-Gierula, M., 2006. Cholesterol-sphingomyelin interactions: a molecular dynamics simulation study. *Biophys. J.* 91, 3756-3767.

Rohit, A., Stapleton, F., Brown, S.H.J., Mitchell, T.W., Willcox, M.D.P., 2014. Comparison of tear lipid profile among basal, reflex, and flush tear samples. *Optom. Vis. Sci.* 91, 1391-1395.

Tiffany, J.M., Todd, B.S., Baker, M.R., 1997. Calculation of the exposed area of the human eye. *Invest. Ophthalmol. Vis. Sci.* 38, 766-766.

Vaknin, D., Kelley, M.S., Ocko, B.M., 2001. Sphingomyelin at the air–water interface. *J. Chem. Phys.* 115, 7697-7704.

Wizert, A., Iskander, D.R., Cwiklik, L., 2014. Organization of lipids in the tear film: a molecular-level view. *PLoS One* 9, e92461.

## Figures

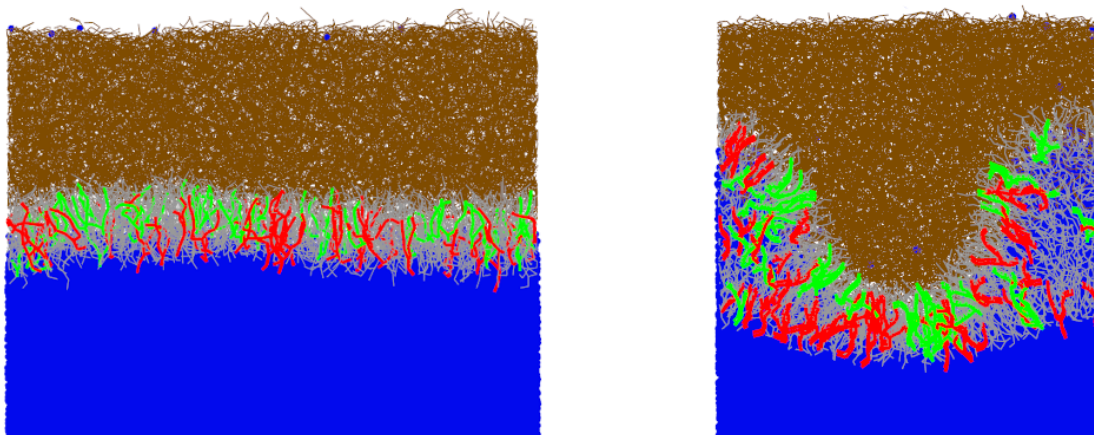


Fig. 1. Typical snapshots of the simulation box taken from simulations at APPL = 0.67 (left) and  $0.45 \text{ nm}^2$  (right). Color coding: red – SM; green - Cer; grey – POPC and POPE; brown – nonpolar lipids; blue – water.

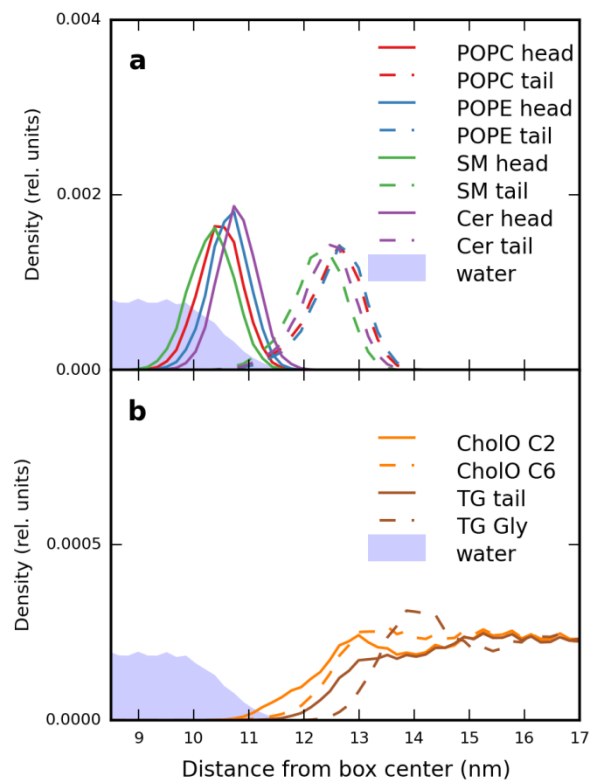


Fig. 2. Density profiles of headgroups and tails of all polar lipids and water (a) and density profiles of non-polar lipids and water (b) calculated at  $APPL = 0.67 \text{ nm}^2$ .

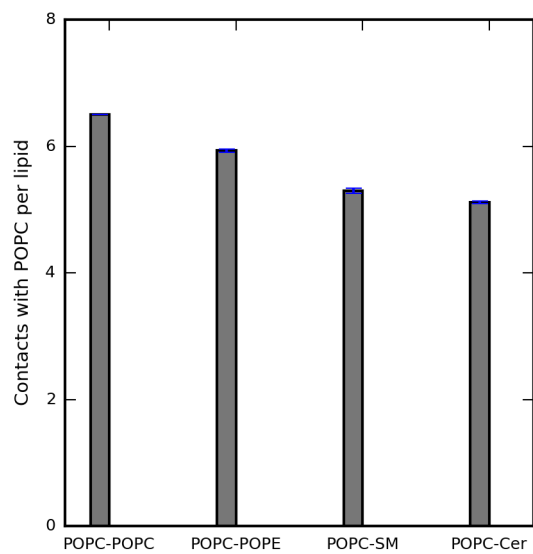


Fig. 3. Average number of contacts between an average POPC molecule and other polar lipid molecules at  $APL=0.67 \text{ nm}^2$ . The cutoff of 0.6 of interatomic distance was employed to define a contact. The analysis was performed employing the Gromacs “mindist” tool with the option “-group”. The data obtained at  $APPL=0.45 \text{ nm}^2$  are shown in supplementary Fig. S2.

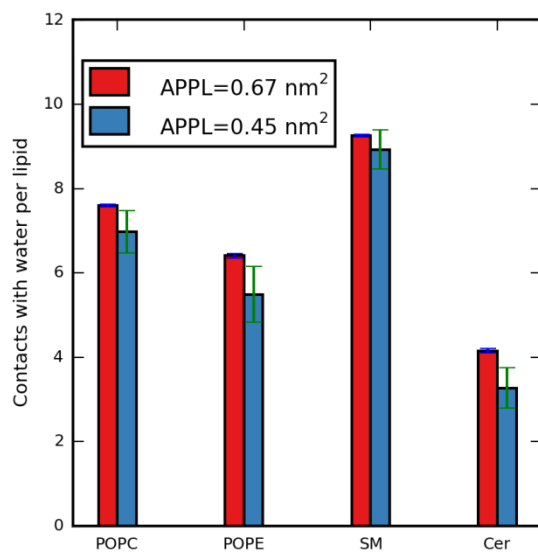


Fig. 4. Average number of contacts between water beads and a polar lipid molecule of a given type at APL=0.67 and 0.45 nm<sup>2</sup>. The cutoff of 0.6 of interatomic distance was employed to define a contact. The analysis was performed employing the Gromacs “mindist” tool with the option “-group” employed.

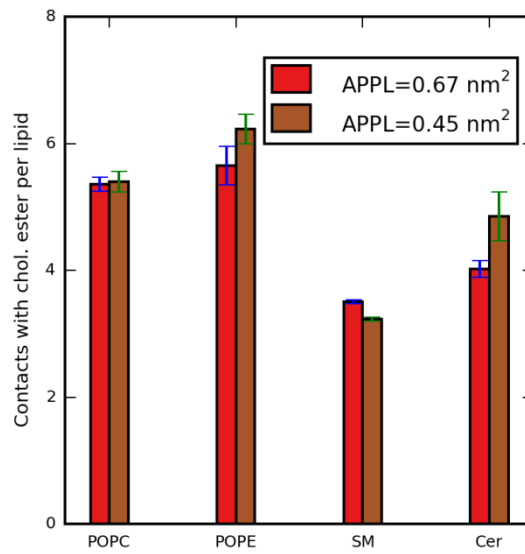


Fig. 5. Average number of contacts between a polar lipid molecules and molecules of cholesterol ester at APL=0.67 and 0.45 nm<sup>2</sup>. The cutoff of 0.6 of interatomic distance was employed to define a contact. The analysis was performed employing the Gromacs “mindist” tool with the option “-group” employed.

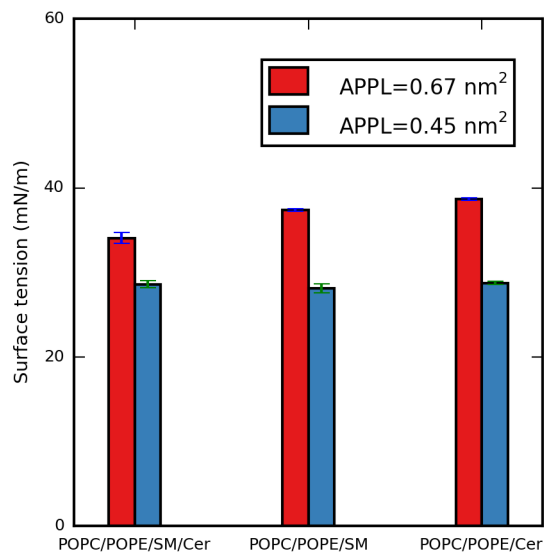


Fig. 6. Surface tension calculated during MD simulations of the TFLL model (the system consisting of POPC/POPE/SM/Cer, together with TG and CE) and two auxiliary systems deficient in either Cer (POPC/POPE/SM) or SM (POPC/POPE/Cer). In the case of the ternary systems, APPL was in fact equal to 0.71 nm<sup>2</sup> for the relaxed and 0.49 nm<sup>2</sup> for the compressed case because these systems were constructed by removal of selected lipids while keeping the simulation box size.

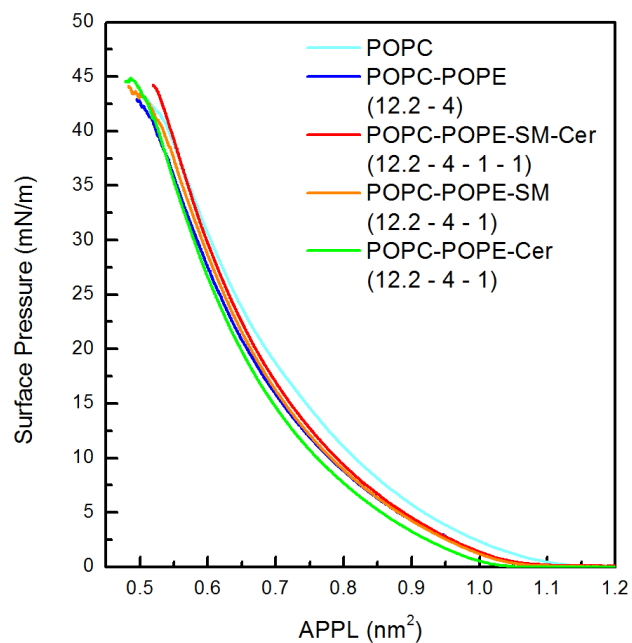


Fig. 7.  $\pi$ -A isotherms measured for quaternary POPC/POPE/SM/Cer and ternary POPC/POPE/SM and POPC/POPE/Cer lipid compositions at physiologically relevant lipid ratios. For comparison, isotherms of POPC/POPE and pure POPC monolayers are shown. Measurements were performed at 310 K.

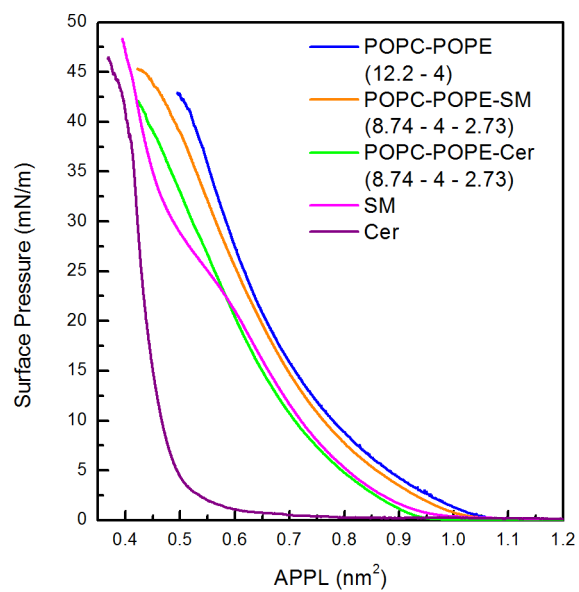


Fig. 8.  $\pi$ -A isotherms measured for lipid systems with the following compositions::  
 POPC/POPE, POPC/POPE/SM, POPC/POPE/Cer, pure SM, and pure Cer. Measurements  
 were performed at 310 K.